The Diffraction of Kelvin Waves and Bores at Coastal Bends

WILLIAM C. SKAMAROCK, JOSEPH B. KLEMP, AND RICHARD ROTUNNO

*National Center for Atmospheric Research, * Boulder, Colorado*

(Manuscript received 11 May 1995, in final form 22 November 1995)

ABSTRACT

Bends in coastal mountain ranges may diffract propagating atmospheric Kelvin waves and trapped coastal currents. Analytic solutions exist for the diffraction of both linear Kelvin waves and linear nonrotating gravity waves. Within the context of the single-layer shallow-water equations, we examine the diffraction of nonlinear gravity waves and bores in a nonrotating reference frame and nonlinear Kelvin waves and coastally trapped bores in a rotating reference frame. The diffraction process can significantly decrease the amplitude of linear and nonlinear waves and bores in the nonrotating reference frame. Unlike for their linear counterpart, however, the diffraction-related amplitude decay for the nonrotating nonlinear waves takes place entirely within the region of the bend and does not produce a continuous decay after the bend. Moreover, theory predicts a critical bend angle at which bore amplitudes will be zero at the wall after propagation around the bend, but shallow-water model simulations do not confirm the existence of the critical angle. For Kelvin waves and trapped bores in the rotating reference frame, we find robust wave and bore propagation around coastal bends in all cases. No critical angles exist for the waves and bores in the rotating reference frame.

1. Introduction

There are many examples of atmospheric flows where topography plays a crucial role in flow evolution. Examples of flows interacting with topographic barriers include marine-layer boundary currents and waves observed on the U.S. West Coast (Dorman 1985, 1987), the southeast Australian coast (Holland and Leslie 1986), and the South African coast (Gill 1977) where coastal mountain ranges act as a barrier, and continental cold air damming with subsequent barrier flow (Bell and Bosart 1988). In these cases the role of a topographic feature is to act as a wall through which the marine layer flow may not pass. The topography is often irregular and may contain significant bends, and in cases involving coastally trapped waves, the bends may act to diffract the waves with a resulting loss in wave amplitude. For example, Reason and Steyn (1992) suggest that the diffraction of solitary Kelvin waves may have been responsible for the cessation of observed trapped waves for the California event of 3–7 May 1982 and in the Australian event of 9–11 November 1982.

Theory exists describing wave diffraction for linear gravity waves (no rotation) and linear Kelvin waves (rotation), but there is little theoretical guidance on the nature of wave diffraction for nonlinear waves and bores including or excluding the effects of rotation. In order to clarify the role wave diffraction can play in the propagation of trapped coastal disturbances, we examine and extend theory for the diffraction of horizontally propagating waves bounded on one side by a wall (barrier) that contains a convex bend. We examine wave diffraction within the context of the single-layer shallow-water equations (SWE). Use of the SWE is appropriate because we are dealing with disturbances that are propagating on a shallow inversion, and existing theory is based on longwave theory. For cases involving bores and gravity currents, the SWE are supplemented with front conditions that specify the relations across the discontinuities in the solutions. We concern ourselves with waves initially propagating parallel to the wall where downstream the wall bends away from the initial propagation vector (convex bend). Where possible we compare theory with numerical simulations of the shallow water equations, and where no theory exists we examine the numerical simulations to determine the diffraction characteristics. Our primary emphasis is to understand the nature of wave diffraction for various wave types and to determine if there are critical bend angles precluding disturbance propagation around the bend, where the critical angle is defined as being the bend angle where wave diffraction results in zero wave amplitude at the wall after the wave is diffracted by the bend. Three general wave types, depicted in Fig. 1, are examined—linear waves, bores, and nonlinear waves of elevation having finite wavelengths that steepen into discontinuities. For these wave types we examine wave diffraction in rotating

* The National Center for Atmospheric Research is sponsored by the National Science Foundation.

Corresponding author address: Dr. William C. Skamarock, NCAR/MMM Division, P.O. Box 3000, Boulder, CO 80307-3000.

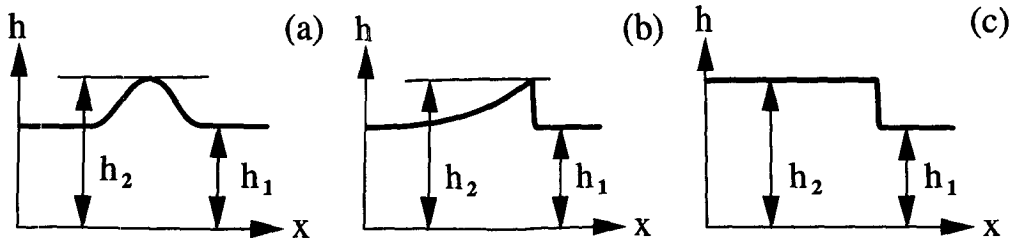

FIG. 1. Wave types: (a) linear wave with $h_2 - h_1 \ll h_1$, (b) single-hump wave with a leading discontinuity, and (c) a bore or hydraulic jump. h_1 is the depth of the quiescent fluid, and in the limit as $h_1 \to 0$ the bore (c) becomes a gravity current.

and nonrotating reference frames. Our primary interest is in the waves with rotation that are trapped by the rotational effects. We examine the nonrotating waves to better understand the rotational case and because over short timescales and space scales the waves with rotation will behave as their nonrotating counterparts.

We begin, in section 2, by reviewing the existing theory for linear wave diffraction in the rotating and nonrotating reference frames. The case of nonlinear breaking waves of finite wavelength is considered in section 3, where a combination of existing linear and nonlinear theory produce reasonable estimates of wave decay associated with the wave-breaking processes. The diffraction of bores, in a nonrotating reference frame, is analogous to the diffraction of shock waves in gasdynamics. In section 4 we modify the gasdynamics theory of shock diffraction to describe bore propagation and compare the theory with numerical simulations of the shallow-water equations. We conclude our consideration of bore diffraction by examining numerical simulations of bores in a rotating reference frame, a case for which no theory exists. A summary and discussion of these results follows in section 5.

2. Linear theory

a. Exact solutions with no rotation

The nonlinear shallow-water equations, including rotational effects, can be written as

$$\frac{du}{dt} + g'\frac{\partial h}{\partial x} - fv = 0, \tag{1a}$$

$$\frac{dv}{dt} + g'\frac{\partial h}{\partial y} + fu = 0, \tag{1b}$$

$$\frac{dh}{dt} + h\left(\frac{\partial u}{\partial x} + \frac{\partial v}{\partial y}\right) = 0, \tag{1c}$$

where

$$\frac{d}{dt} = \frac{\partial}{\partial t} + u\frac{\partial}{\partial x} + v\frac{\partial}{\partial y}.$$

In (1), u and v are the horizontal velocities, h is the height of the free surface, g' is the reduced gravity, f is the Coriolis parameter, and (x, y, t) are the two spatial and temporal coordinates, respectively. The nonlinear shallow-water equations (1) can be linearized and, with $f = 0$ and no mean flow, reduce to the linear wave equation

$$h_{tt} + g'h_1\nabla^2 h = 0, \tag{2}$$

where h_1 is the depth of the quiescent fluid, and h is now the perturbation height field $h = h_2 - h_1$ (see Fig. 1). On the walls, a no-normal-flow boundary condition results in

$$\frac{\partial h}{\partial n} = 0, \tag{3}$$

where n is the direction normal to the wall. Sommerfeld (1896) derived an exact solution to (2) and (3) for the problem of diffraction of an incident electromagnetic wave impinging upon a perfectly conducting wedge of arbitrary angle. The wedge geometry is given in Fig. 2, and we are interested in the magnetic-field component of an electromagnetic field in which the angle of incidence is zero. Sommerfeld's solution is given in terms of a complex integral and can be found, along with an asymptotic solution, in Landau and Lifshitz (1984, 305–307). The asymptotic solution for the diffraction region II in Fig. 2 is

$$\frac{h(r, \phi)}{h_0} = H(r, \phi)\exp(-i\omega t),$$

where h_0 is the incident wave amplitude. The dimensionless wave amplitude is

$$H(r, \phi) = \frac{2\pi}{\gamma(2\pi kr)^{1/2}}\exp\left[i\left(kr + \frac{\pi}{2}\right)\right] \times \frac{\sin(\pi^2/\gamma)}{\cos(\pi^2/\gamma) - \cos[\pi(\phi + \pi)/\gamma]}, \tag{4}$$

where $\gamma = \theta_b + \pi$ and the wavenumber $k = 2\pi/L$. The asymptotic analysis and (4) are valid when

$$\cos(\pi^2/\gamma) - \cos[\pi(\phi + \pi)/\gamma] \gg 1/kr.$$

Figure 3 shows the exact and asymptotic solutions for a 45° bend in the wall. The diffraction produces both constructive and destructive interference, and along

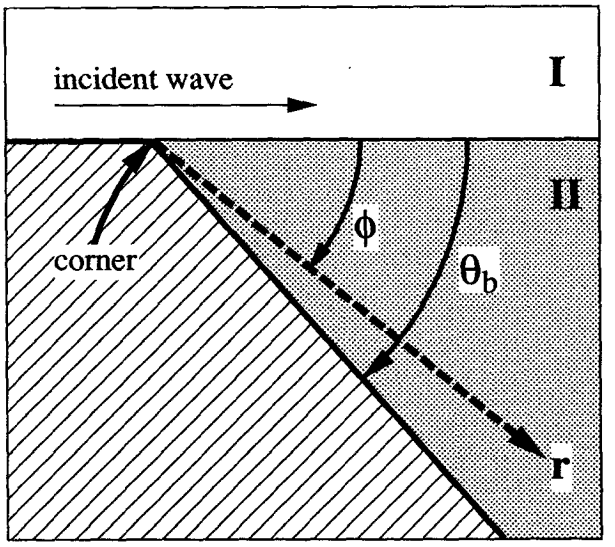

FIG. 2. The wedge geometry in (ϕ, r) coordinates in the wedge-diffraction theory. The wedge is the region with diagonal lines, and the bend angle is denoted θ_b. The incident wave travels from left to right in region I, and the shadow-region is region II.

the wall the solution decays asymptotically with $h \sim (kr)^{-1/2}$. This solution also can be used for continuous waveforms by Fourier decomposing the waveform and treating each mode separately. Thus, any mode will exhibit a $(kr)^{-1/2}$ decay with waves having higher wavenumbers (shorter wavelengths) decaying more rapidly. Also, the theory predicts that there is no critical angle for wave diffraction, that is, there is no angle at which the wave amplitude becomes zero after the corner (except at infinite distance from the corner).

b. Exact solution with rotation

The waveform for the linear wave with rotation is the same as in Fig. 1a except that the wave decays exponentially away from the wall $(+y)$ with the decay factor being $\exp[-yf/(g'h_1)^{1/2}]$. Packham and Williams (1968) found an exact closed-form solution for the linearized shallow-water equations that included rotation and assumed no mean flow and an incident wave with a sinusoidal waveform exhibiting exponential decay away from the wall. They also derived an asymptotic solution that is a function of the bend angle θ_b (see Fig. 2) and the hyperbolic tangent of the ratio of the frequency of the reference frame rotation to that of the approaching wave, $\lambda_0 = \tanh(f/\omega)$. Unlike the nonrotating case, there is no wave decay after the bend and only wave decay at the bend. Given this behavior, Packham and Williams solution can be expressed as a transmission coefficient T (the ratio of the along-wall wave amplitude after the bend to the wave amplitude before the bend) for the asymptotic solution

$$T = \left(\frac{\cosh 2\pi\lambda_0/\gamma - \cos\pi^2/\gamma}{\cosh 2\pi\lambda_0/\gamma + \cos\pi^2/\gamma}\right)^{1/2} \tanh\frac{\pi\lambda_0}{\gamma},$$

where again $\gamma = \theta_b + \pi$ and the solution is valid for large kr and $\omega > f$. Figure 4 shows the transmission coefficient for two wave frequencies $\omega > f$. As in the case with no rotation, there are no critical angles wherein the wave amplitude is zero (for $\omega/f \to \infty$, $T \to 0$ asymptotically). For $\omega < f$ the transmission coefficient $T = 1$; there is no decay because Poincare waves, responsible for the energy flux from the Kelvin

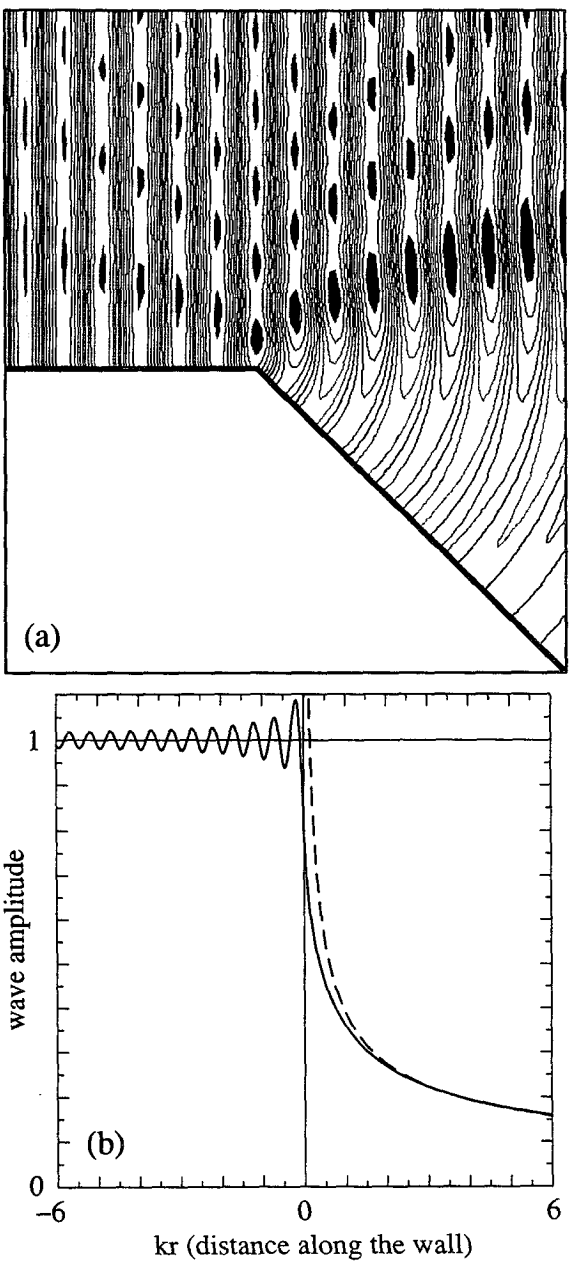

FIG. 3. (a) The perturbation height field (h/h_0) from the exact solution (Sommerfeld 1896) for the linear wedge-diffraction problem without rotation. The contour interval is 0.2 and absolute magnitudes greater than 1 are in black. (b) $|\eta|$ along the wall from the exact solution along with the perturbation solution valid after the corner.

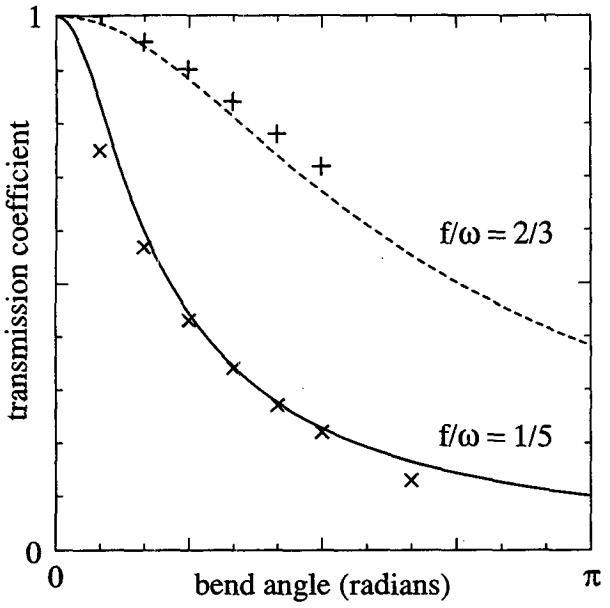

FIG. 4. Asymptotic solution for the wedge diffraction problem with rotation. The ×s and +s are results from numerical shallow-water simulations using a smooth bend where the radius of curvature of the bend is greater than the wavelength.

waves, are limited to frequencies less than f, and hence the Poincare waves are evanescent (examples of Poincare waves can be found in Figs. 6 and 11 depicting diffraction of the single-hump wave and bore, respectively).

Packham and Williams' exact solution was derived for a sharp corner. Also shown in Fig. 4 are the transmission coefficients obtained from simulations using a curvilinear coordinate shallow-water model (described in appendix A). The bend is not sharp in the model, and we have found that the bend's radius of curvature has little effect on the transmission coefficient. In the simulations we also find that, in contrast to the case without rotation, there is no wave decay except in the immediate vicinity of the bend. The Kelvin wave history is propagation with constant amplitude before the bend, decay with propagation around the bend, and propagation with a constant, smaller, amplitude after the bend.

3. Nonlinear theory and simulations for finite-length discontinuous waves

Given adequate time, nonlinear effects will cause a wave of elevation (depression) to steepen and break on its upstream (downstream) side, forming a bore with the height profile of the single-hump wave in Fig. 1b. Whitham (1974, 42–48) has shown that if the speed of the bore is approximated as a quadratic function, the single-hump wave has the time-varying solution

$$\sqrt{h_2} - \sqrt{h_1} = \sqrt{\frac{2A}{t}}, \qquad (5)$$

where A is the area of the hump over the undisturbed value $\sqrt{h_1}$ and is constant in time, that is,

$$A = \frac{1}{\sqrt{g'}} \int_0^L (\sqrt{h_2} - \sqrt{h_1})\, dx.$$

Next we address the wave diffraction resulting from the propagation of this wave around a bend with and without rotation.

a. Case with no rotation

Whitham's analysis shows that the single-hump wave will decay as $t^{-1/2}$ after it sharpens into a discontinuity, where in this case we speak of the decay of the quantity $\sqrt{h_2} - \sqrt{h_1}$. There is no theory that predicts the wave decay after the bend. We would, however, expect that the single-hump wave will decay after the bend by the same mechanism, producing decay before the bend (assuming that it retains its discontinuity), and that there should be an additional decay associated with diffraction of the finite-wavelength wave by the bend. We have performed shallow-water simulations with the curvilinear coordinate model and present the results from two simulations in Fig. 5. The initial waves have wavelengths that differ by a factor of four in the two simulations, and there are three distinct regions in the time–height plots in both cases. At early times, before the wave reaches the bend, the wave steepens into a bore and decays as approximately $t^{-1/2}$. Well after the bend the wave again decays at a constant rate that is generally greater than $t^{-1/2}$, with the two cases shown

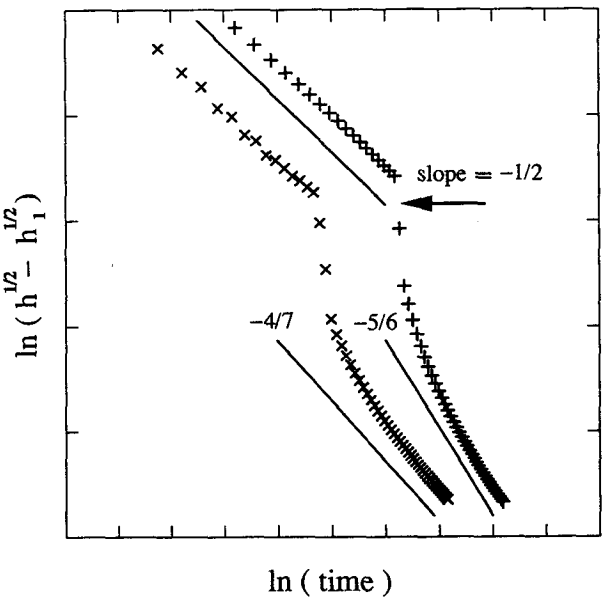

FIG. 5. Time–height plot for the single-hump wave with no rotation for two simulations. The data plotted at equal time intervals on the log–log plot. The case with the smaller decay rate after the bend has an initial wavelength four times that of the other case.

in Fig. 5 exhibiting asymptotic decay rates of approximately $t^{-5/6}$ and $t^{-4/7}$, where the shorter initial-wavelength disturbance has the higher decay rate. Finally, during propagation around the bend there is additional wave decay associated with the discontinuous nature of the wave and its bore-like character. In the bend region the decay rates are greater than those in the asymptotic-decay regions upstream and downstream of the bend. Both the theory and simulations of bore diffraction (see section 4) show decay in the region of the bend but not after the bend, and the discontinuous single-hump wave is consistent with bore diffraction in that it has its largest decay rate at the bend.

As in the previous case, we find that the bend's radius of curvature has little effect on the wave evolution away from the bend region. The simulations also suggest that the wave decay after the bend is not sensitive to the wave amplitude, but rather it is most sensitive to the wavelength of the diffracting wave and the bend angle, and we find that the waves with shorter wavelengths decay at higher rates after the bend. For very short waves ($\omega \gg f$), the diffraction process is complex and the decay rates often do not approach a steady rate even after $10f^{-1}$.

b. Case with rotation

For the rotational case, the waveform at the wall is the same as in Fig. 1b, except now the wave is confined to the vicinity of the wall. Figure 6 depicts a single-hump wave before diffraction by the bend. The initial waveform is linear with exponential decay in y. As the wave steepens, the discontinuous wave front away from the wall bends behind the front at the wall. Even with this complex structure, the single-hump wave still exhibits decay proportional to $t^{-1/2}$ before encountering the bend.

We might expect the wave to decay as $t^{-1/2}$ after the bend according to Whitham's analysis embodied in (5) if the single-hump discontinuous wave behaves in an analogous fashion to the linear waves because the linear analysis for rotational linear waves predicts that there is no decay associated with the bend except that confined to the region of the bend. Figure 7 is a time–height plot of a shallow-water simulation of a single Kelvin wave that steepens into a discontinuity. As in the case without rotation, there are three regions of interest in the wave evolution. First, the wave decays approximately as $t^{-1/2}$ in the region before the bend after bore formation. After the bend the wave again decays approximately as $t^{-1/2}$, as suggested by analogy with linear theory. The wave behavior is complex in the region of the bend. While there appears to be significant decay associated with the bend, there also is an adjustment where the wave returns to the $t^{-1/2}$ decay and recovers the lost amplitude. The behavior at the corner is a transient, temporary phenomena that has little effect on downstream evolution. In this case as in the other cases, we find no appreciable quantitative differences in the solutions when altering the curvature radius of the bend angle, although the solution in the region of the bend can change considerably; the $t^{-1/2}$ decay remains both before and after the bend.

4. Bores

a. Theory without rotation

Whitham (1959, 1974, chapter 8) develops a theory for the diffraction of shock waves in the context of gasdynamics based on diffraction theory from geometrical optics. The shock-diffraction theory is generalizable to a bore by substituting the shallow-water equations for the compressible Euler equations and by substituting the bore conditions (relating the flows ahead of and behind the bore) for the shock conditions. Whitham (1974, 270) describes the generalization, and based on this generalization we derive the bore-diffraction theory in appendix B.

The principal result of the theory can be found in Fig. 8, which can be directly interpreted as a plot of the incident bore strength versus the critical bend angle, where the bore strength is expressed in terms of a bore Froude number $F = U/a$, U is the speed of the bore, the wave speed $a = (g'h_2)^{1/2}$, h_2 is the depth of the fluid behind the bore, and the critical angle is in radians. From Fig. 8 it can be immediately discerned that if the approaching bore is close to a gravity current ($h_1/h_2 \rightarrow 0$, $F \rightarrow \sqrt{2}$), then the critical angle is greater than 180° and no physically realizable critical angle exists for the case of a sharp bend (a discontinuous corner).

The theory also provides for the calculation of bore decay from diffraction, using Fig. 8, for bend angles less than the critical angle. For a bore of incident Froude number F_0 and critical angle θ_c, its post-bend Froude number will be $F = F(\theta_c - \theta)$, where θ is the bend angle, and $F(\theta_c - \theta)$ is the Froude number associated with $\theta_c - \theta$ in Fig. 8.

b. Simulations without rotation

Numerical model simulations of a bore propagating around bends of 15° and 45° are plotted against the theory in Fig. 9 where F is plotted as a function of F_0. While the theory appears reasonably accurate for the 15° case, it is noticeably in error in the 45° case where predicted Froude numbers are often less than one-half the observed values. This inaccuracy is not entirely unexpected. In the gasdynamics analysis of shock-wave diffraction, Skews (1967) compared Whitham's theory with experiments and found that the theory also is relatively inaccurate at low Mach number and high bend angles (see Figs. 5a and 5c in Skews, which plotted M_w, the wall Mach number after the bend, versus M_0). The gravity-induced bores are analogous to low Mach number shocks because the highest Froude number that can be produced using gravity alone as the motive force is $\sqrt{2}$ and the Froude number is analogous to the Mach number.

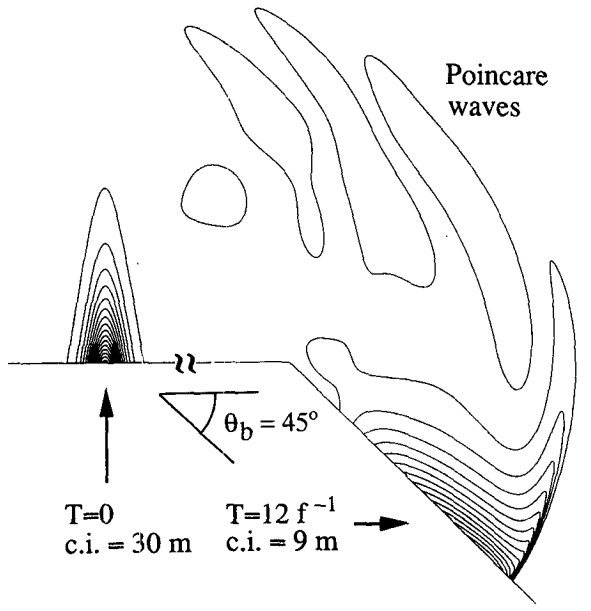

FIG. 6. Height field for single-hump wave in the case with rotation. The initial condition is the linear Kelvin wave, and the more complex cross-shore structure develops as the nonlinear effects become important. Diffraction has little effect on the wave amplitude and structure.

Further examination of Fig. 9 suggests that the critical angle predicted in the theory is not realized in the simulations. For a 45° angle, an incident bore of Froude number less than approximately 1.06 should not propagate around the 45° bend. However, the numerical results show a bore with an incident Froude number of approximately 1.03 propagating around the bend with a Froude number of 1.01 after the bend. This is also found in the experimental data of Skews for the shock-diffraction problem. Figure 7 in Skews shows a critical angle predicted by theory of ~110° for $M_0 = 1.5$, whereas the data show no critical angle at all. Moreover, Skews states that in none of his experiments did the shock separate from the wall or show zero shock strength ($M \rightarrow 1$).

Another feature of the shallow-water solutions for the bore is a drop in the height field and an acceleration of the fluid in the vicinity of the corner in the flow behind the bore, with two such cases depicted in Figs. 10a and 10b.

If the flow behind the bore is subcritical with respect to the corner (Fig. 10a), as determined by examining the Froude number of the flow $F = u_2/(g'h_2)^{1/2}$, then both the acceleration and height drop are qualitatively understood by analogy to potential flow solutions around a sharp corner (see Batchelor 1967, 410–412). In these potential flow solutions the flow accelerates in the vicinity of the corner (with infinite velocity at the corner, but we can take any streamline as the wall), and the pressure drops as the fluid accelerates. In the shallow water simulations the drop in the height field is analogous to the pressure drop, and in both cases the fluid accelerates. However, the potential flow solutions are nondivergent, whereas the shallow-water flow around the bend is not, and thus the analogy is not complete (we find that the flow diverges in the vicinity of the bend).

If the flow is supercritical (Fig. 10b), an expansion fan forms in the flow directly after the bend behind the leading bore, similar to those discussed by Winant et al. (1988), Samelson (1992), and Whitham (1974, section 6.17) in the context of gasdynamics. The fans are characterized by a drop in the height field and an acceleration of the flow as it rounds the bend. Downstream of the bend, the leading bore sets the height to which the flow around the bend must recover, and this height is determined by the diffraction process. If the accelerated flow around the bend in the expansion fan is supercritical relative to the flow behind the leading bore, a hydraulic jump (a second bore) must form if the supercritical expansion fan flow is to return to a subcritical flow dictated by the leading bore. This second bore is evident in Fig. 10b. For large bend angles (>135°) and large incident Froude numbers ($F_0 \rightarrow \sqrt{2}$), the expansion fan and second bore can interact with the leading bore resulting in separation of the leading bore from the wall.

We do not believe that the shallow water model solutions containing a second bore are physically realistic with respect to the second bore. In the derivation of the bore conditions (which are implicitly satisfied by the advective formulation of the SWE numerical model) the upper layer is assumed to be passive, and it also is assumed that there is no shear between the flow ahead of the bore and the passive upper layer; the velocity of

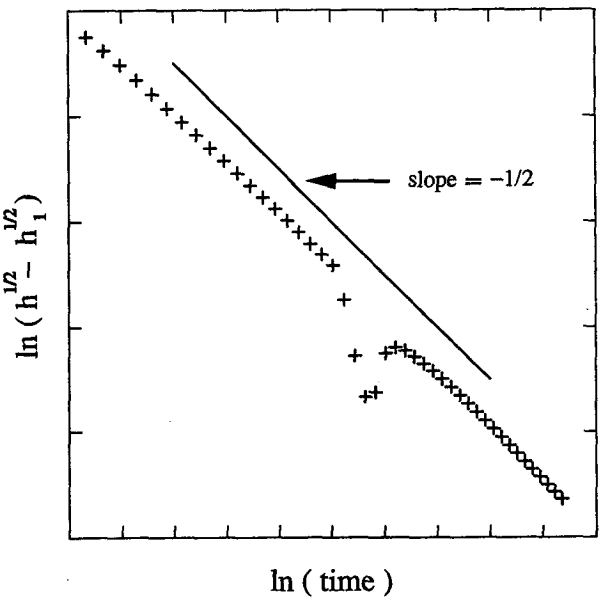

FIG. 7. Time–height plot for the single-hump wave with rotation with the data plotted at equal time intervals of $0.72f^{-1}$ on the log–log plot.

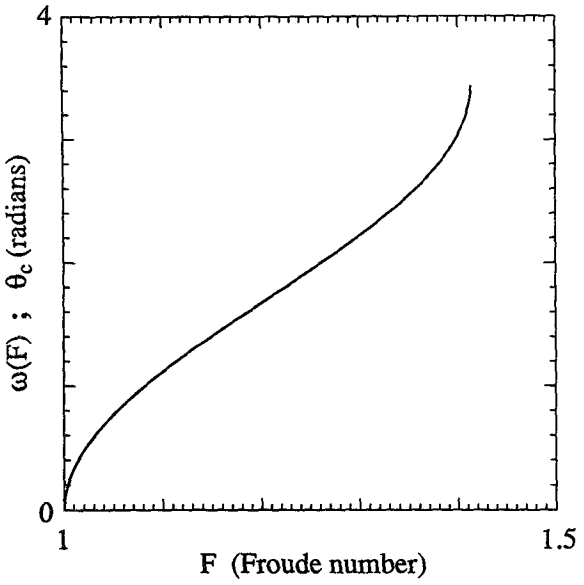

FIG. 8. Plot of $\omega(F)$ (or the critical angle θ_c) versus the Froude number F from the bore-diffraction theory (no rotation).

the lower and upper layers ahead of the bore are assumed to be equivalent. However, there is a large velocity ahead of the second bore in these simulations and a large shear exists between the lower layer and the passive upper layer. Thus, the assumptions that are used to derive the bore conditions are not satisfied and the evolution of this jump is not simulated correctly. However, while the SWE model solutions appear physically unrealistic with respect to the second bore, we believe that the evolving expansion fan may affect the leading bore in some cases. A more sophisticated model would be needed to examine this interaction.

c. *Simulations with rotation*

We do not have theory for the diffraction of bores in a rotating environment. Theory for weakly nonlinear waves, with irregular coastlines possessing bends with curvature radii much greater than the Rossby radius, are considered by Clarke (1977). He finds that wave diffraction can produce significant phase changes but little amplitude decay. Clarke does not consider bores or strongly nonlinear disturbances. Our simulations, using the shallow-water equations, strongly suggest that the bores will experience minimal decay under all conditions because the flows are always turned back into the wall because of the rotation. As was the case for the single-hump waves, the time period for reestablishment of steady flow is less than $3f^{-1}$ to $5f^{-1}$ (see Fig. 7).

For a steady boundary current with a leading bore, the simulations show that if the radius of curvature of the bend is equal to or greater than the Rossby radius ($R_0 = U/f$), the bore will propagate smoothly around the bend with little adjustment evident. As the radius of curvature decreases, an adjustment is observed such that the bore decays as it propagates around the bend but later returns to its original strength. In the case of a sharp corner, depicted in Fig. 11, the bore and wall current will separate at the corner and reattach downstream. There is a second weak bore behind the leading bore in Fig. 11 that is similar to the second bore that forms in the case without rotation, however, its scale is much smaller. In the cases with rotation it requires larger bore strengths, larger bend angles, and smaller bend curvature to form the bores, and in no case that we have simulated does it result in permanent separation of the primary bore because the flow inexorably turns into the wall and reestablishes a wall current and bore. As in the case without rotation, we do not believe that the second bore is physically realistic, but in the case with rotation the second bore plays no role in the evolution of the leading bore.

5. Discussion

The wave-diffraction results for the nonrotating reference frame can be summarized as follows. Linear waves are diffracted by the bend and decay as $x^{-1/2} \sim t^{-1/2}$ after the bend as a result of the diffraction. Waves that steepen into discontinuities resemble a single hump (Fig. 1b) where the quantity $\sqrt{h_2} - \sqrt{h_1}$, a measure of the wave amplitude, will decay as $t^{-1/2}$ before the bend, as $>t^{-1/2}$ after the bend, and will experience an additional decay at the bend as a result of their discontinuous nature. Bores decay as they propagate around the bend but do not decay afterward.

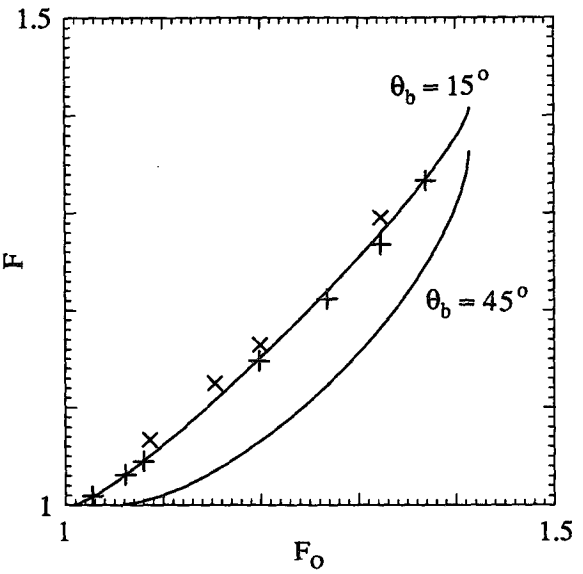

FIG. 9. Froude number of the incident bore (F_0) versus the along-wall Froude number of the diffracted bore (F) after propagation around a smooth bend with no rotation. The solid line represents theory and the points are results from shallow-water model simulations for a 15° (×) and a 45° (+) bend angle.

Generally, the numerical model simulations agree with theory. However, the theory for bore diffraction is not accurate; it is poor for anything but small bend angles (in the small Froude number regime) and its prediction of critical angles is not verified by the simulations where separation occurs based on effects not included in the geometrical-optics theory of Whitham (1959). The nonrobust nature of the bore-diffraction theory is shared by the analogous shock-diffraction theory (at low Mach numbers) as highlighted by the experiments of Skews (1967).

Wave diffraction in a rotating reference frame is dramatically different than that in the nonrotating reference frame. In all cases, the diffraction effects are localized to the region of the bend and there is no continuous decay after the waves pass the bend. For monochromatic linear waves, wave diffraction results in wave decay for $\omega/f > 1$, that is, for short, high-frequency waves. After leaving the influence of the bend there is no further decay in contrast with the $x^{-1/2}$ decay in the nonrotating case. As in the nonrotating case, there is no critical angle. For the single-hump wave there is decay associated with wave breaking (decay $\sim t^{-1/2}$), and this decay rate is found both before and after the bend. There is wave decay associated with the leading discontinuity propagating around the bend. There is no theory for bore diffraction in the rotating reference frame, and the numerical simulations strongly suggest that there is no appreciable decay associated with diffraction at the bend. In the rotating frame, model simulations agree with the existing theory for wave diffraction for linear waves and wave propagation for the single-hump wave before and after the bend. Finally, there is no evidence of permanent wave separation in any simulations in the rotating reference frame in contrast to the observed bore separation in the nonrotating frame and, while secondary bores do form in the rotating case, they play no role in the evolution of the leading bore. Overall, the rotational theory and simulations suggest that diffraction can significantly affect small-scale wave evolution for linear waves, where small scale implies $L < U/f$ and $T < 1/f$. Diffraction does not affect strongly nonlinear waves (bores) and large-scale waves (linear or nonlinear).

The diffraction theory and shallow-water model simulations presented herein have encompassed linear and strongly nonlinear waves. We have not considered the

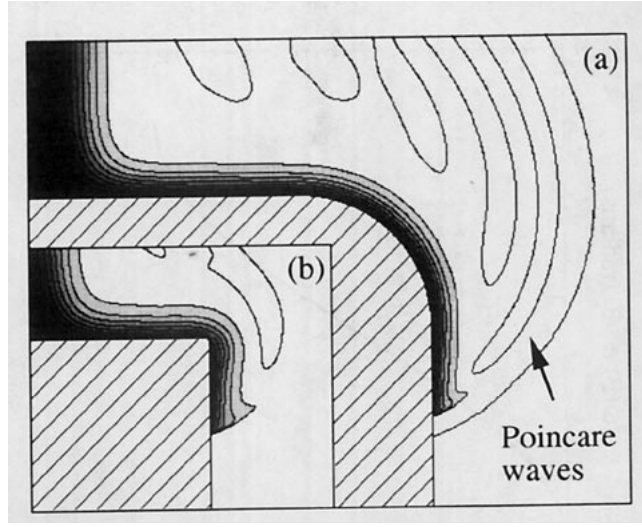

FIG. 11. Height field for bores propagating around a convex bend of 90° in a rotating framework with bend radius of curvature (a) greater than the Rossby radius and (b) less than the Rossby radius. The length scales are approximately equal in (a) and (b), with the dam being much closer to the bend in (b). The height field ahead of the bore is 500 m and the contour interval is 50 m, with darker shading indicating a greater depth.

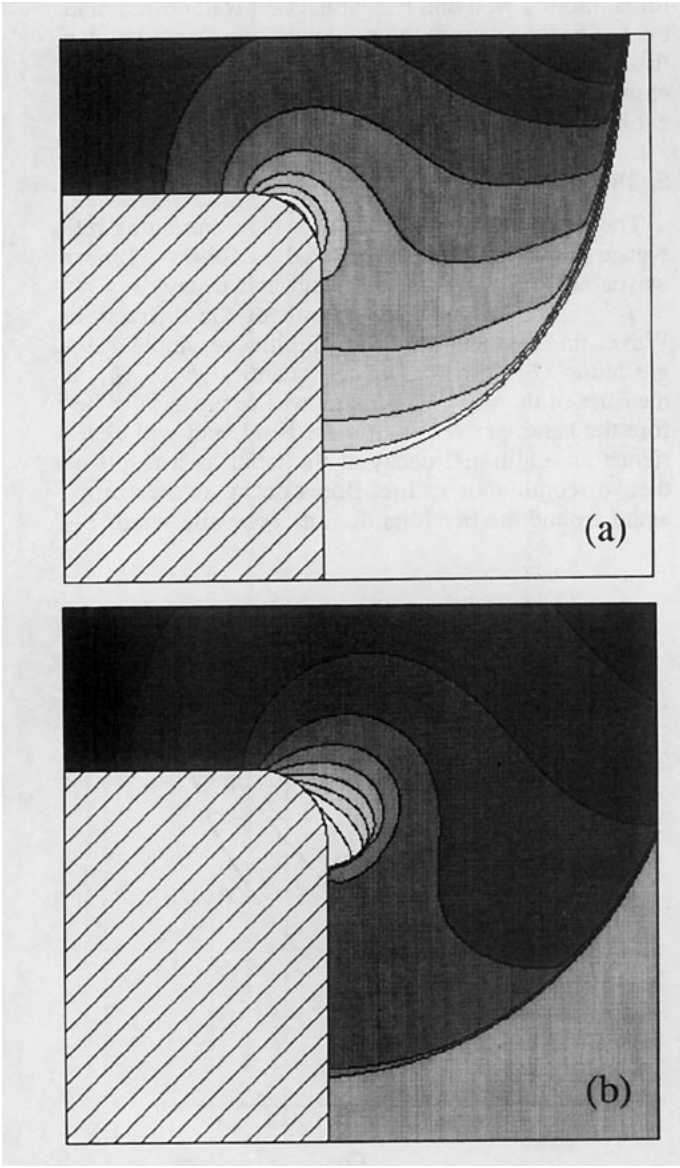

FIG. 10. Height field from the shallow water simulations showing bores after propagation around a bend with an angle of 90° for incident Froude numbers of (a) 1.09 and (b) 1.18: h_1 = 500 m and the contour interval for (a) c.i. = 30 m and (b) c.i. = 60 m. The leading contour is 500 m in both plots. An expansion fan and second bore are found immediately after the bend in (b).

weakly nonlinear solitary waves, where a solitary wave is a single nonlinear translating wave that does not change in shape and amplitude (its solitary nature traditionally resulting from a balance between nonlinear steepening and wave dispersion). Reason and Steyn (1992) suggest that rotational solitary waves (Kubokawa and Hanawa 1984) have been observed in both the 3–7 May 1982 California case and the 9–11 November 1982 Australian case and that the waves separated from the coast at a coastal bend and ceased propagating as a result of wave diffraction. They argue that the critical angle, predicted in the analysis of Miles (1977) for the propagation of nonrotating solitary waves about a bend, is applicable to the observed coastally trapped propagating waves. We do not believe that the nonrotating theory of Miles can be applied to the rotating case because both linear and strongly nonlinear waves diffract very differently in the rotating and nonrotating cases; the nonrotating theory does not possess the correct dynamics to capture diffraction in the rotating case. We also observe: 1) it has not been demonstrated that the observed waves are examples of the rotating solitary wave described by Kubokawa and Hanawa; 2) the rotating solitary wave is a perturbation solution on a mean current, and the first question to be considered with respect to diffraction is whether the current makes it around the bend should the current exist; 3) the theory of Miles is based on the geometrical-optics theory of Whitham. Experiments and simulations have shown that the critical angles predicted by the theory do not exist in either shock dynamics (Skews 1967) or bores (theory, shallow-water simulations in this paper). Miles theory for solitary waves, including the result concerning the critical angle, has not been verified observationally, experimentally, or numerically, thus it is not clear if the critical angle prediction is accurate.

Acknowledgments. This research was supported in part by the Office of Naval Research Grant N00014-94-F-0032.

APPENDIX A

Numerical Model Formulation

The curvilinear coordinate version of the shallow-water model follows the formulation of Dietachmayer (1992). The shallow-water equations (1) are transformed from the coordinate system (x, y, t) to the system (ϵ, η, t), with the new equations being

$$u_t + u_E \frac{\partial u}{\partial \epsilon} + v_E \frac{\partial u}{\partial \eta} + \frac{g'}{\sqrt{G}}\left(\frac{\partial h}{\partial \epsilon}\frac{\partial y}{\partial \eta} - \frac{\partial h}{\partial \eta}\frac{\partial y}{\partial \epsilon}\right) - fv = 0,$$

$$v_t + u_E \frac{\partial v}{\partial \epsilon} + v_E \frac{\partial v}{\partial \eta} + \frac{g'}{\sqrt{G}}\left(\frac{\partial h}{\partial \eta}\frac{\partial x}{\partial \epsilon} - \frac{\partial h}{\partial \epsilon}\frac{\partial x}{\partial \eta}\right) + fu = 0,$$

$$h_t + u_E \frac{\partial h}{\partial \epsilon} + v_E \frac{\partial h}{\partial \eta} + \frac{h}{\sqrt{G}}\left(\frac{\partial u}{\partial \epsilon}\frac{\partial y}{\partial \eta} - \frac{\partial u}{\partial \eta}\frac{\partial y}{\partial \epsilon} + \frac{\partial v}{\partial \eta}\frac{\partial x}{\partial \epsilon} - \frac{\partial v}{\partial \epsilon}\frac{\partial x}{\partial \eta}\right) = 0,$$

where

$$u_E = \frac{1}{\sqrt{G}}\left(u\frac{\partial y}{\partial \eta} - v\frac{\partial x}{\partial \eta}\right),$$

$$v_E = \frac{1}{\sqrt{G}}\left(v\frac{\partial x}{\partial \epsilon} - u\frac{\partial y}{\partial \epsilon}\right),$$

and

$$\sqrt{G} = \frac{\partial x}{\partial \epsilon}\frac{\partial y}{\partial \eta} - \frac{\partial x}{\partial \eta}\frac{\partial y}{\partial \epsilon}.$$

The transformed equations are differenced on a B grid so that the discrete system is invariant with respect to rotation. A wall (barrier) is specified along one boundary of the domain ($\eta = 0$ boundary), and the other boundaries are open and use gravity-wave radiating boundary conditions (Klemp and Wilhelmson 1978). The wall boundary is specified at the height points, and the boundary condition needed to solve the height equation along the wall is that the velocity normal to the wall is zero. The time differencing is leapfrog. Both fourth- and second-order filtering (in ϵ and η) have been used along with a second-order dissipation in x and y [see Dietachmayer and Droegemeier (1992) for the formulation of the ∇^2 terms] with constant eddy viscosity or hyper viscosity used in all applications. The dissipation in the model is used to keep the computations stable, and the solutions presented here have been found to be insensitive to the form of the dissipation and the values of the eddy viscosity.

APPENDIX B

Bore-Diffraction Theory

The bore-diffraction theory is a modification of the shock-diffraction theory of Whitham (1974, chapter 8) and we follow his outline. The theory is based on diffraction theory from geometric optics combined with the 1D gasdynamics equations and shock relations. We modify this by substituting the shallow water equations and bore relations into the theory, leaving the geometric optics theory as is. We begin by briefly outlining the geometric optics theory (Whitham 1974, section 8.4) and conclude by presenting the shallow water equations and bore relations necessary to complete the theory. In presenting the optics theory, we use the shallow-water terminology in place of the gasdynamics terminology.

For the 2D problem, the bore positions and rays orthogonal to the bore make up an orthogonal coordinate system in which the theory is developed. This coordinate system is depicted in Fig. B1. Whitham derives a relationship between the normalized width of the ray channel A and the normalized speed of the bore F (the

Froude number $F = U/a$, where U is the bore speed, the longwave speed $a = (g'h)^{1/2}$, and h is the height of the fluid behind the bore). In Fig. B1 the increment $d\alpha$ denotes the change in the bore position in time $dt = d\alpha/a$, thus the distance traveled is $Udt = Fd\alpha$ and the line element for $d\alpha$ is $Fd\alpha$. Correspondingly, the line element for $d\beta$ is $Ad\beta$. Next, consider the curvilinear quadrilateral $PQRS$ in Fig. B1 with corners (α, β), $(\alpha + \delta\alpha, \beta)$, $(\alpha, \beta + \delta\beta)$, and $(\alpha + \delta\alpha, \beta + \delta\beta)$. Defining $\theta(\alpha, \beta)$ to be the angle between a ray and a fixed direction, the change in the ray angle θ from P to S is

$$\delta\theta = \frac{QR - PS}{PQ} = \frac{1}{F}\frac{\partial A}{\partial \alpha}\delta\beta,$$

which can be written as

$$\frac{\partial \theta}{\partial \beta} = \frac{1}{F}\frac{\partial A}{\partial \alpha}. \tag{B1}$$

Similarly, given the orthogonality of the system, the change in angle for the β curves leads to

$$\frac{\partial \theta}{\partial \alpha} = \frac{1}{A}\frac{\partial F}{\partial \beta}. \tag{B2}$$

The general problem is to determine θ, F, and A as a function of α and β, and the next step in this process is to determine the relationship $A = A(F)$. We will consider this step in a moment, but first, having that relationship, we can write the characteristic form of (B1) and (B2) as

$$\left(\frac{\partial}{\partial \alpha} \pm c\frac{\partial}{\partial \beta}\right)\left(\theta \pm \int \frac{dF}{Ac}\right) = 0, \tag{B3}$$

where c is a function of F given by

$$c(F) = \sqrt{\frac{-F}{AA'}},$$

and $A' = dA/dF$. The Riemann invariants for (B3) are

$$\theta \pm \int \frac{dF}{Ac} = \text{const on } d\beta/d\alpha = \pm c.$$

Considering a wall with a single convex bend of θ_w (see Fig. 2), and defining

$$\omega(F) = \int_1^F \frac{dF}{Ac}, \tag{B4}$$

the definition of the Riemann invariant along the wall leads directly to the relation

$$\omega(F) = \omega(F_0) - \theta_b, \tag{B5}$$

where F_0 is the Froude number of the approaching bore, and F is the Froude number of the bore after it has passed around the bend. This is the result we desire because it directly reveals the bore strength after propagation around the bend; given the function $\omega(F)$, F_0, and θ_b, F is uniquely determined using (B5).

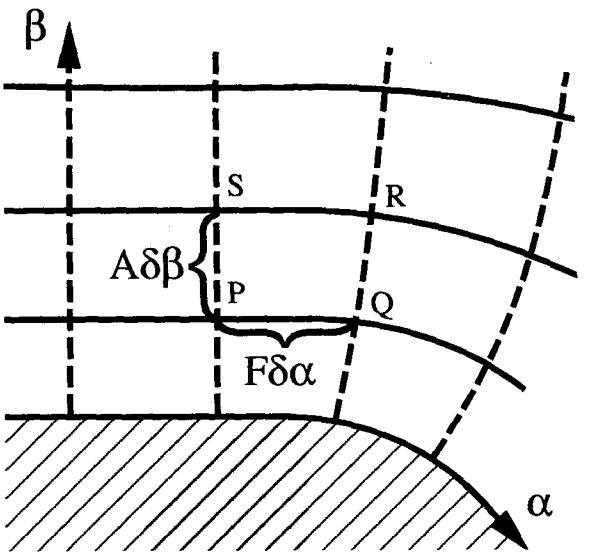

FIG. B1. Coordinate system for the bore-diffraction theory.

What remains is to determine $\omega(F)$, and to do this we must determine $A = A(F)$. It is here that the shallow water equations and bore conditions are substituted for the gasdynamics equations and shock relations. Again we follow Whitham (1974, section 8.1). First, the characteristic equations for 1D flow in x with a cross section slowly varying in x is derived. The addition of a slowly varying cross section alters the height equation (1c) such that it becomes

$$h_t + uh_x + hu_x + hu\frac{A'(x)}{A(x)} = 0, \tag{B6}$$

where $A(x)$ is the cross-sectional area perpendicular to the flow. The characteristic equation for (1a) and (B6) is

$$\left[\frac{\partial}{\partial t} + (u \pm a)\frac{\partial}{\partial x}\right](u \pm 2a) + au\frac{A'}{A} = 0, \tag{B7}$$

where $a = (g'h)^{1/2}$.

We do not use the standard bore conditions (Rayleigh 1914), but rather we use the bore conditions derived in Klemp et al. (1994, 1995) that give a solution similar to the standard bore conditions when h_1 is of the same order as h_2 and that converge to Benjamin's result (1968) in the gravity current limit where $h_1 \to 0$ (the standard bore condition predicts an infinite speed or a vanishing bore height as $h_1 \to 0$). The bore conditions from Klemp et al. are

$$U = u_1 + \left[g'h_2\frac{2h_2}{h_1 + h_2}\right]^{1/2}$$

and

$$u_2 = u_1 + \frac{h_2 - h_1}{h_2}\left[g'h_2\frac{2h_2}{h_1 + h_2}\right]^{1/2}.$$

In the reference frame where u_1 is zero and h_1 is constant, we can recast the bore conditions as

$$h = \frac{h_1 F^2}{2 - F^2} \tag{B8}$$

and

$$u = 2aF\left(1 - \frac{1}{F^2}\right), \tag{B9}$$

where u and h are the dependent variables. Following Whitham, the bore conditions (B8) and (B9) are substituted into the characteristic equation (B7) (using the positive characteristic), which results in an equation relating A to F:

$$\frac{F}{F^2 - 1}\lambda(F)\frac{dF}{dx} + \frac{1}{A}\frac{dA}{dx} = 0, \tag{B10}$$

where

$$\lambda(F) = \left(3F - \frac{1}{F} + 1\right)\cdot\left(1 + \frac{1}{F}\right) - \left(F - \frac{1}{F} + 2\right)\frac{1 - F^2}{F(2 - F^2)}.$$

The form of (B10) is identical to (8.25) in Whitham (1974) except for different λs. Also, in the gasdynamics analysis Whitham assumes that $u_t/(u + a)$ and $h_t/(u + a)$ are small compared to the other terms in the characteristic equation and discards them. We have included these terms with the approximation $u_t = Uu_x$ and $h_t = Uh_x$ and find better agreement with the model results.

Finally, (B10) can be used to eliminate A from (B4), which leads to the definition of ω

$$\omega(F) = \int_1^F \left(\frac{\lambda(F)}{F^2 - 1}\right)^{1/2} dF. \tag{B11}$$

Figure 8 is a plot of ω as a function of F and also represents a direct solution of (B5).

REFERENCES

Batchelor, G. K., 1967: *An Introduction to Fluid Dynamics.* Cambridge University Press, 615 pp.

Bell, G. D., and L. F. Bosart, 1988: Appalachian cold-air damming. *Mon. Wea. Rev.*, **116,** 137–161.

Benjamin, T. B., 1968: Gravity currents and related phenomena. *J. Fluid Mech.*, **31,** 209–248.

Clarke, A. J., 1977: Wind-forced linear and nonlinear Kelvin waves along an irregular coastline. *J. Fluid Mech.*, **83,** 337–348.

Dietachmayer, G. S., 1992: Application of continuous dynamic grid adaption techniques to meteorological modeling. Part II: Efficiency. *Mon. Wea. Rev.*, **120,** 1707–1722.

——, and K. K. Droegemeier, 1992: Application of continuous dynamic grid adaption techniques to meteorological modeling. Part I: Basic formulations and accuracy. *Mon. Wea. Rev.*, **120,** 1675–1706.

Dorman, C. E., 1985: Evidence of Kelvin waves in California's marine layer and related eddy generation. *Mon. Wea. Rev.*, **113,** 827–839.

——, 1987: Possible role of gravity currents in northern California's coastal summer wind reversals. *J. Geophys. Res.*, **92,** 1497–1506.

Gill, A. E., 1977: Coastally trapped waves in the atmosphere. *Quart. J. Roy. Meteor. Soc.*, **103,** 431–440.

Holland, G. J., and L. M. Leslie, 1986: Ducted coastal ridging over S. E. Australia. *Quart. J. Roy. Meteor. Soc.*, **112,** 731–748.

Klemp, J. B., and R. Wilhelmson, 1978: The simulation of three-dimensional convective storm dynamics. *J. Atmos. Sci.*, **35,** 1070–1096.

——, R. Rotunno, and W. C. Skamarock, 1994: Propagation of atmospheric gravity currents along a coastal barrier. Preprints, *Sixth Conf. on Mesoscale Processes,* Portland, OR, Amer. Meteor. Soc., 497–500.

——, ——, and ——, 1995: Propagation of bores in a Boussinesq environment. Preprints, *10th Conf. on Atmospheric and Oceanic Waves and Stability,* Big Sky, MT, Amer. Meteor. Soc., 73–74.

Kubokawa, A., and K. Hanawa, 1984: A theory of semigeostrophic gravity waves and its application to the intrusion of a density current along a coast. Part 2. *J. Oceanogr. Soc. Japan,* **40,** 260–270.

Landau, L. D., and E. M. Lifshitz, 1984: *Electrodynamics of Continuous Media,* 2d ed. Pergamon Press, 460 pp.

Miles, J. W., 1977: Diffraction of solitary wave. *Z. Agnew. Math. Phys.*, **28,** 889–902.

Packham, B. A., and W. E. Williams, 1968: Diffraction of Kelvin waves at a sharp bend. *J. Fluid Mech.*, **34,** 517–529.

Rayleigh, Lord, 1914: On the theory of long waves and bores. *Proc. Roy. Meteor. Soc.*, **90,** 324–328.

Reason, C. J., and D. G. Steyn, 1992: The dynamics of coastally trapped mesoscale ridges in the lower atmosphere. *J. Atmos. Sci.*, **49,** 1677–1692.

Samelson, R. M., 1992: Supercritical marine-layer flow along a smoothly varying coastline. *J. Atmos. Sci.*, **49,** 1571–1584.

Skews, B. W., 1967: The shape of a diffracting shock wave. *J. Fluid Mech.*, **29,** 297–304.

Sommerfeld, A., 1896: Mathemtische theorie der diffraktion. *Math. Ann.*, **47,** 314–317.

Whitham, G. B., 1959: A new approach to the problems of shock dynamics. Part II: Three-dimensional problems. *J. Fluid Mech.*, **5,** 369–386.

——, 1974: *Linear and Nonlinear Waves.* Wiley and Sons, 636 pp.

Winant, C., C. Dorman, C. Friehe, and R. Beardsley, 1988: The marine layer off northern California: An example of supercritical channel flow. *J. Atmos. Sci.*, **45,** 3588–3605.